PHYSICAL REVIEW B VOLUME 25, NUMBER 2 15 JANUARY 1982

Empirical band calculations of the optical properties of *d*-band metals. III. Rh and Pd

R. Lässer* and N. V. Smith
Bell Laboratories, Murray Hill, New Jersey 07974
(Received 17 February 1981)

Band-structure calculations for Rh and Pd have been performed by a second-principles approach using a combined interpolation scheme. From these bands the imaginary part of the dielectric function ϵ_2 in the energy range $\hbar\omega \leq 25$ eV has been calculated with full inclusion of momentum matrix elements and spin-orbit effects. The band-by-band decompositions of ϵ_2 are presented, and structures are identified with transitions between specific bands in $\vec{k}$ space. Agreement with experiment is found to be good, and identifications are offered for the principal experimental structures. Furthermore, ϵ_2 values assuming constant matrix elements for both direct and nondirect transitions have been calculated to assess the influence of the matrix elements and to test the direct-transition model.

I. INTRODUCTION

Over the last few years the electronic properties of Rh and Pd have been the subject of a number of papers.[1-22] Particular attention has been paid to the electronic behavior of Pd, which has been studied experimentally by the de Haas–van Alphen effect,[1] optical spectroscopy,[2] photoemission spectroscopy (angle-integrated[3-5] and angle-resolved[6-8]), Compton scattering[9] and thermomodulated reflectance,[10] and theoretically using band-structure computation methods[3,9,11-15] with a nonrelativistic or relativistic, non-self-consistent or self-consistent approach. This paper continues the earlier optical-absorption calculations of the noble metals[23] and the alloy system $Ag_{1-\chi}Cd_{\chi}$.[24] The imaginary part ϵ_2 of the dielectric function for Rh and Pd has been calculated with full inclusion of momentum matrix elements and spin-orbit effects in the region $\hbar\omega \leq 25$ eV. So far, the experimental ϵ_2 spectra have been compared only with joint-density-of-states[2,14] (JDOS) calculations where the influence of the variation of the matrix elements is neglected. The calculation procedure is described briefly in Sec. II. Results are compared with experiment in Sec. III and the band-by-band decomposition is presented in Sec. IV.

II. COMPUTATIONAL METHOD

The imaginary part ϵ_2 of the dielectric constant was calculated from the standard equation:

$$\epsilon_2^d(\hbar\omega)=\frac{e^2}{3\pi m^2\omega^2}\sum_{f,i}\int_{BZ} d^3k \; |P_{fi}|^2 \times\delta(E_f(\vec{k})-E_i(\vec{k})-\hbar\omega). \quad (1)$$

The superscript denotes that we consider only direct ($\vec{k}$-conserving) transitions. Equation (1) is a one-electron theoretical expression, and local-field effects and electron-hole interactions are neglected.

The computational procedure follows basically the same steps described in earlier papers.[23-25] Very briefly, it involves fitting the parameters of a combined interpolation scheme, solving the eigenvalue problem of a 42×42 Hamiltonian matrix to obtain the energy values $E_i(\vec{k})$ and $E_f(\vec{k})$ of the initial and final states, and computing the momentum matrix elements $\vec{P}_{fi}$. The 42×42 matrix consists of a 16×16 plane-wave block, a 5×5 tight-binding d block, and a 5×16 hybridization submatrix. This 21×21 matrix is doubled and elements added to include spin-orbit effects.[26] To obtain the 18 parameters of the combined interpolation scheme the energy eigenvalues were fitted to the results of a first-principles band-structure calculation using a nonlinear least-squares method. Table I lists the 18 parameters of the combined interpolation scheme for Rh and Pd. The values were obtained by fitting 36 relativistic augmented-plane-wave eigenvalues at the high-symmetry points Γ, X, L, W, and Σ calculated by Christensen.[14,20] The rms errors were 0.064 and 0.032 Ry for Rh and Pd, respectively. The momentum matrix elements were calculated by differentiation of the Hamiltonian matrix.[27]

TABLE I. Parameters of the combined interpolation scheme obtained by fitting the Rh and Pd eigenvalues of Refs. 14 and 20, respectively (all values are given in rydberg).

	Rh	Pd
E	0.6285	0.4882
Δ	−0.0053	−0.0065
A_1	0.044 13	0.020 59
A_2	0.004 78	0.002 35
A_3	0.008 22	0.007 14
A_4	0.015 55	0.008 87
A_5	0.006 55	0.003 74
A_6	0.020 09	0.010 21
α	0.011 68	0.011 45
V_{000}	0.2828	0.1295
V_{111}	0.0970	0.0750
V_{200}	0.0902	0.0695
V_{220}	−0.0224	−0.0017
V_{311}	0.2231	0.1529
V_{222}	0.2709	0.2446
R	0.396	0.320
S	1.368	1.636
B_t	1.954	1.905
B_E	1.954	1.905
ξ	0.012	0.015
E_F	0.717	0.558

Results for $\bar{\epsilon}_2^d(\hbar\omega)$ have also been calculated from Eq. (1) by treating the momentum matrix elements as constant. This quantity is (apart form a factor involving ω^2) the JDOS which merely expresses the total number of possible direct transitions between occupied and unoccupied bands at a certain photon energy. Comparison between ϵ_2^d and $\bar{\epsilon}_2^d$ therefore, shows the influence of the momentum matrix elements.

So far only direct interband transitions (where $\vec{k}$ vector and energy are conserved) have been considered. Spicer[28] has postulated a nondirect interband transition model where $\vec{k}$-vector conservation does not pertain or is unimportant. In this model ϵ_2 can be calculated from the density of states (DOS), $N(E)$, by computation of the following integral:

$$\bar{\epsilon}_2^n \sim \frac{1}{\omega^2} \int_{E_F-\hbar\omega}^{E_F} N(E)N(E+\hbar\omega)dE \ . \qquad (2)$$

In Eq. (2) it is assumed that the transition matrix elements are constant. In the cases of $\bar{\epsilon}_2^n$ and $\bar{\epsilon}_2^d$ the theoretical results have to be scaled to the experimental data. Therefore, only the frequency dependence of the curves is important, whereas in the case of $\epsilon_2^d(\hbar\omega)$ the absolute values as well as the energy dependence are significant.

III. RESULTS AND COMPARISON WITH EXPERIMENT

This section compares the main structures of the theoretical and experimental ϵ_2 curves. A detailed analysis of the band-by-band contributions to the ϵ_2 function is given in the following section.

A. Rhodium

Figure 1 shows the theoretical ϵ_2^d results for Rh together with the experimental values of Weaver *et al.*[18,29] The experimental ϵ_2 results of Rh show shoulders at the low energies 1.2, 2.8, 5.4 eV, a minimum at 9.0 eV, and a broad plateau in the energy range between 10 and 21 eV with three structures at 11.6, 14.6, and 19.3 eV. The agreement with the theoretical ϵ_2^d curve is good with regard to both positions and intensities of structues. Absolute comparison in the extreme low-energy region is difficult because the experimental data contain both the intraband and the interband contributions, whereas the computation procedure includes only

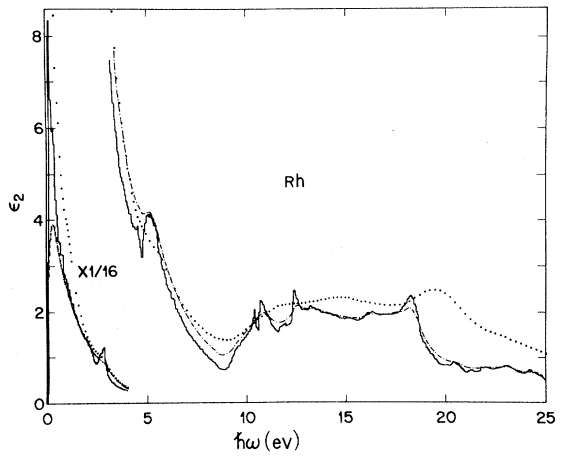

FIG. 1. Calculated ϵ_2 spectrum (solid line) of Rh in comparison with experimental values (dots) of Refs. 18 and 29. Dot-dashed curve: ϵ_2 values after convolution of the solid line with a Lorentzian function of FWHM = 0.4 eV.

interband transitions. The theoretical ϵ_2^d shows peaks at 2.8 and 5.4 eV, a pronounced minimum at 8.8 eV, and a broad plateau in the range $10 < \hbar\omega < 19$ eV. Three main structures within this plateau region at $\hbar\omega = 10.8$, 12.5, and 18.4 eV occur $\sim 1-2$ eV lower than those seen in experiment. This discrepancy could be removed, or much reduced, by an empirical adjustment to the band stucture which pushes the appropriate final-state bands to higher energies. This is discussed further in Sec. IV.

The features in the theoretical ϵ_2^d curves are much sharper than those observed experimentally. The smearing is presumably due to lifetime broadening of the initial and final electron states. The dot-dashed curve in Fig. 1 represents an attempt to simulate these effects by convolving the ϵ_2^d results with a Lorentzian of full width at half maximum (FWHM) equal to 0.4 eV. This is equivalent to assuming that the sum of the lifetimes of the initial and final states may be treated as constant.

B. Palladium

Figure 2 shows the theoretical ϵ_2^d results and the experimental data for Pd published by Weaver[2] and Weaver *et al.*[16,17,29] The same notation is used as in Fig. 1. The experimental data show a change of slope at 1.3 eV, a well-defined shoulder at ~ 4.3 eV, a minimum at ~ 8.9 followed by a plateau region having three broad structures at about 10.0, 15.0, and 20.4 eV. The overall behavior is, therefore, similar to that for Rh.

The solid line is the result of the ϵ_2^d calculation for Pd. The overall agreement with experiment is good. The change of slope at 1.3 eV and the peak at 4.2 eV occur at about the same energies as in experiment. The most noteworthy feature is the grouping of structures in the theoretical ϵ_2^d curve at 20.5 eV. The discussion in the next section will show that these peaks lie too close to each other due to difficulties in the fitting method. Therefore, intensity should be distributed to the regions both below and above ~ 20.4 eV, resulting in better agreement. The dot-dashed curve in Fig. 2 is the result of a convolution of the ϵ_2^d data with a Lorentzian of FWHM = 0.4 eV to simulate lifetime effects.

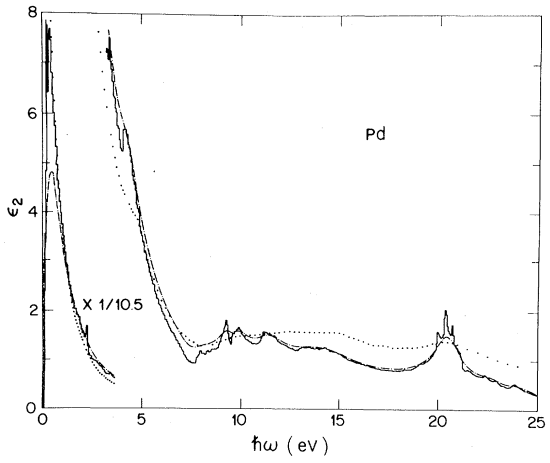

FIG. 2. Calculated ϵ_2 spectrum (solid line) of Pd in comparison with experimental values (dots) of Refs. 16, 17, and 29. Dot-dashed curve: ϵ_2 values after convolution of the solid line with a Lorentzian function of FWHM = 0.4 eV.

IV. THE BAND-BY-BAND DECOMPOSITION

This section gives a more detailed identification of the structures in the ϵ_2^d curves of Figs. 1 and 2. The total ϵ_2^d spectra are decomposed into the partial contributions $\epsilon_2^d(i \rightarrow f)$ from initial band i into final band f. The superscript d (for direct transitions) will be omitted. Because of the multitude of structures, we shall discuss only those features in the partial ϵ_2 spectra which are prominent or which can be related to experimentally observed structures.

A. Rhodium

The band structure of Rh obtained by the parameters of Table I and the parial ϵ_2 spectra belonging to these bands are shown in Figs. 3 and 4, respectively. The filled circles in Fig. 3 represent the first-principles eigenvalues calculated by Christensen.[20] Below the Fermi level the second-principles scheme fits the first-principles results quite well, but the agreement deteriorates in the region above 14 eV. Figure 4 is divided into seven parts, each one showing the possible partial ϵ_2 spectra from the occupied bands into empty final bands with the band index running from 4 to 10. The bands are numbered in increasing order of energy.

In Fig. 4 we can distinguish two main groupings of structures. Below 8.5 eV contributions are due to transitions into final bands 4—6, whereas in the region $8.5 \leq \hbar\omega \leq 21.5$ eV, final bands 7—9 are

mainly involved. This accounts for the minimum at ~ 8.8 eV, followed by an edge which is attributable to the onset of transitions between bands 4—7.

The strong peak at ~ 0.2 eV arises from transitions between bands 3 and 4 near X in the region close to where both bands cut the Fermi level. These transitions are possible because the d bands are hybridized. The change of slope in the experimental data at ~ 1.2 eV (see Fig. 1) originates partly from the strong intensity decrease connected with transitions from band 5 into band 6 and from band 4 into bands 5 and 6. Figure 3 shows that those transitions contributing to the $\epsilon_2(4\rightarrow 5)$ and $\epsilon_2(4\rightarrow 6)$ are possible in large regions of $\vec{k}$ space. They do not occur in the near neighborhood of X and L, because there band 4 is unoccupied, or at Γ, because bands 5 and 6 lie below the Fermi level. The 1.2-eV slope change in the experimental data cannot, therefore, be associated with any high-symmetry critical point. The sharp dropoff of the $\epsilon_2(4\rightarrow 5)$ spectrum at ~ 2.3 eV originates from the maximum energy difference between bands 4 and 5 near the midpoint between W and L.

The hump in the experimental ϵ_2 data at 2.9 eV arises from the peaks in the partial spectra $\epsilon_2(3\rightarrow 5)$ and $\epsilon_2(3\rightarrow 6)$. These transitions occur mainly at and near L and in the direction Σ. The peak in the $\epsilon_2(3\rightarrow 5)$ spectrum is sharp because the two bands 3,5 are parallel at L (see arrow in Fig. 3). The maximum of the $\epsilon_2(1\rightarrow 6)$ spectrum at 5.2 eV is responsible for the feature in the experimental data at 5.4 eV and is due to transitions from band 1 into 6 in the Σ direction. These transitions are drawn as an arrow in Fig. 3.

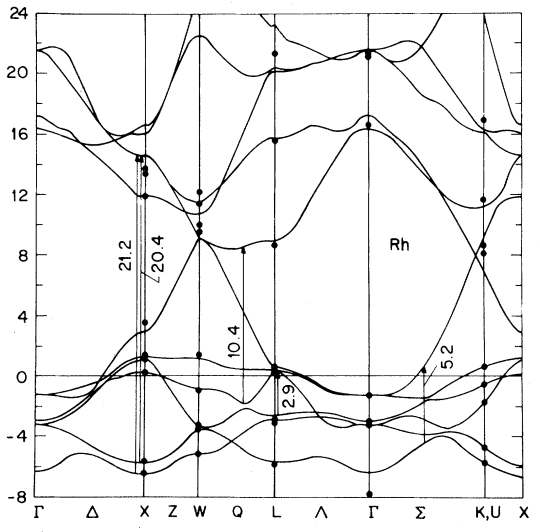

FIG. 3. Band structure of Rh obtained with the parameters of Table I. The dots represent the first-principle eigenvalues calculated by Christensen (Ref. 20), (All numbers are given in eV.)

Let us turn to the structures above the edge starting at about 9 eV. As stated above, the edge itself is due to the onset of transitions between bands 4 and 7. The three sharp theoretical structures at 10.4, 10.8, and 12.5 eV arise from the peaks of the partial spectra $\epsilon_2(4\rightarrow 7)$, $\epsilon_2(3\rightarrow 7)$, and $\epsilon_2(2\rightarrow 7)$, respectively. The first peak is due to transitions in the region between W and L, where bands 3 and 4 approach one another (see arrow in Fig. 3). The second peak (10.8 eV) may be associated with the K, U point. The third peak (12.5 eV) occurs mainly near W in the Q direction.

The maximum of the ϵ_2^d spectrum at 18.4 eV (Fig. 1) is mainly due to the structures in the partial spectra $\epsilon_2(2\rightarrow 8)$, $\epsilon_2(3\rightarrow 8)$, and $\epsilon_2(4\rightarrow 8)$. The sharp peak of the $\epsilon_2(2\rightarrow 8)$ curve arises from transitions in $\vec{k}$ space near L in the direction Q, where bands 2 and 8 are nearly parallel. Transitions at W and L are the cause of the two peaks in the $\epsilon_2(3\rightarrow 8)$ spectrum at ~ 14.1 and ~ 18.3 eV, respectively. The $\epsilon_2(4\rightarrow 8)$ upper edge at ~ 18.6 eV can be understood in terms of transitions in the Λ direction. The peaks of the $\epsilon_2(2\rightarrow 9)$ and $\epsilon_2(1\rightarrow 9)$ spectra at 20.4 and 21.2 eV are due to transitions at X and in the direction Δ. Both transitions are shown in Fig. 3 by arrows. This figure shows further that the fitting scheme has difficulties in reproducing the first-principles higher bands at the correct energy, as mentioned earlier. For example, band 9 is too high relative to the first-principles results at X and band 8 is somewhat low in energy at Γ and in the direction Λ. Therefore, the peaks of the partial spectra $\epsilon_2(2\rightarrow 9)$ and $\epsilon_2(1\rightarrow 9)$ should be shifted to lower energy by 1.1 eV, whereas the humps of the $\epsilon_2(4\rightarrow 8)$ spectrum at ~ 18.6 eV should be transferred to slightly higher energies. As a result of both shifts more intensity relative to the ϵ_2^d curve of Fig. 1 is produced in the region 19.0—20.5 eV, which would go some way towards improivng agreement with experiment. The most effective adjustment, however, to bring about agreement between theory and experiment would be to "stretch" the unoccupied theoretical bands 7 and 8 to higher energies. The need for such a stretch is well established in the case of Cu,[30] and appears to apply also in the case of Au.[23,31]

Our analysis of the "plateau" region may be summarized as follows. The lower edge of the plateau at ~ 9 eV is due to the onset of transitions

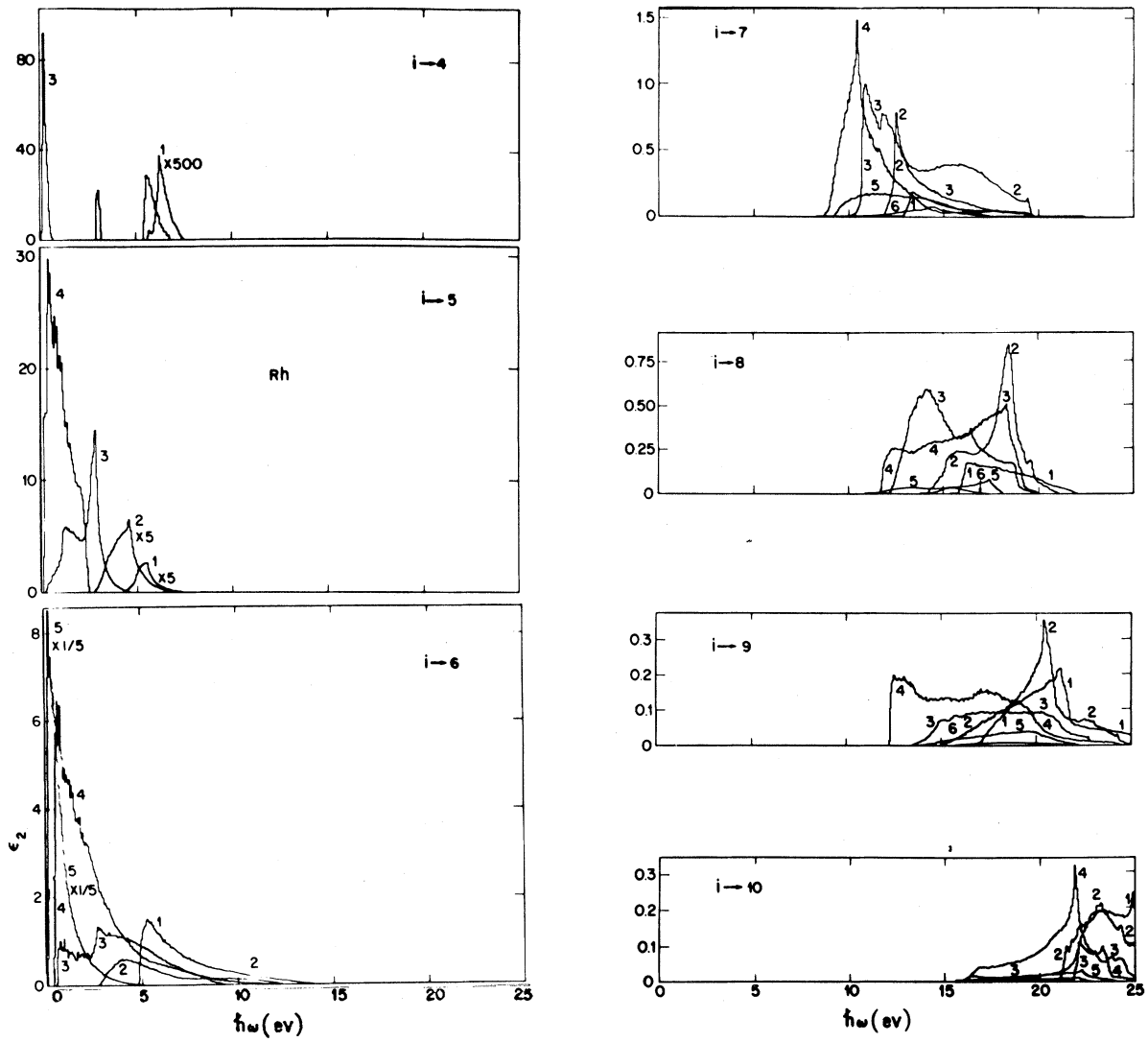

FIG. 4. Partial $\epsilon_2(i \rightarrow f)$ spectra of Rh for transitions from the initial band i into the final band f.

into band 7. The upper edge at ~ 20 eV or thereabouts is due to the termination of transitions to band 8. Structures within the plateau can be identified with individual band pairs involving final states in bands 7 or 8. Overall alignment between the theoretical and experimental plateau could be improved by an empirical stretching of bands 7 and 8 on the energy scale.

B. Palladium

The band structure of Pd obtained using the parameters of Table I is shown in Fig. 5, and the partial ϵ_2 spectra calculated with these bands are shown in Fig. 6. The filled circles in Fig. 5 represent the eigenvalues calculated by Christensen.[14] Figure 6 shows that the ϵ_2^d values presented in Fig. 2 below 7.5 eV are mainly due to transitions into the final bands 5,6 whereas those above are due to transitions into bands $f \geq 7$. The cause of the minimum at 7.5 eV is the significant separation of these two regions.

The sharp peak of the $\epsilon_2(4 \rightarrow 5)$ spectrum at 0.3 eV arises from transitions near X, where both bands cut the Fermi surface, and near and at L, where bands 4 and 5 are just below and above the Fermi level, respectively. The broad feature of the $\epsilon_2(3 \rightarrow 5)$ spectrum at 0.5 eV can be identified with transitions at X. The $\epsilon_2(4 \rightarrow 6)$ spectrum shows a

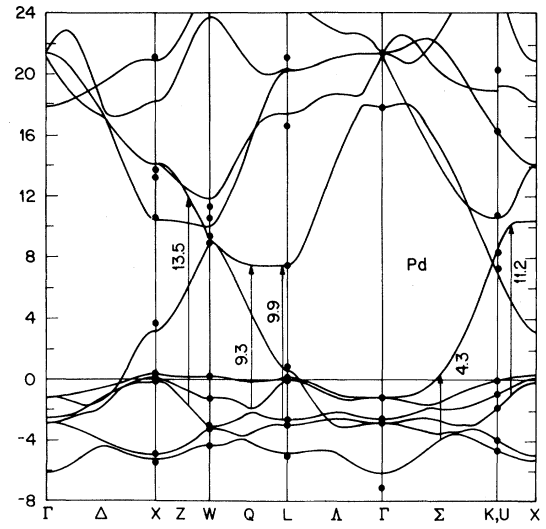

FIG. 5. Band structure of Pd obtained with the parameters of Table I. The dots represent the first-principle eigenvalues calculated by Christensen (Ref. 14). (All numbers are given in eV.)

maximum at about 0.6 eV due to transitions mainly at L. The structures of the $\epsilon_2(3\rightarrow 6)$ spectrum at ~ 1.0 and 2.8 eV arise from transitions in the Δ, Λ, and Σ directions. The shoulder in the experimental curve (Fig. 2) at ~ 4.3 eV coincides with the maximum of the $\epsilon_2(1\rightarrow 6)$ spectrum and can be identified by transitions from band 1 into band 6 in the Σ direction (see arrow in Fig. 5).

The maxima of the partial spectra $\epsilon_2(4\rightarrow 7)$, $\epsilon_2(3\rightarrow 7)$, and $\epsilon_2(2\rightarrow 7)$ are primarily responsible for the structures in the ϵ_2^d curve of Fig. 2 in the range $9 \leq \hbar\omega \leq 12$ eV. Transitions indicated in Fig. 5 by an arrow from band 4 into band 7 in the region between W and L, are responsible for the prominent peak of the partial $\epsilon_2(4\rightarrow 7)$ spectrum at 9.3 eV. Transitions between band 3 and 7 at L and at points between U and X contribute mainly to the two peaks of the spectrum at ~ 9.9 and 11.2 eV, respectively, and are indicated as arrows in Fig. 5.

The $\epsilon_2(i\rightarrow 8)$ spectra show sharp and strong features in the region $19.5 \leq \hbar\omega \leq 22.0$ eV. The hump in the ϵ_2 $(3\rightarrow 8)$ spectrum at ~ 13.5 eV is due to transitions in the region between X and W (see arrow in Fig. 5). The very sharp peaks at 20.1 and 20.4 eV are due to transition from band 3 and 2 into band 8 at L, respectively. The partial ϵ_2 spectra of transitions into the final band 9 show only broad structures with little intensity. The strong peaks in the $\epsilon_2(4\rightarrow 10)$ and $\epsilon_2(3\rightarrow 10)$ spectra at ~ 20.4 and 22.4 eV are due to transitions at L and in the region between W and L, respectively.

Figure 6 shows that the theoretical sharp features at and around 20.5 eV in Fig. 2 arise mainly from contributions of the partial spectra $\epsilon_2(2\rightarrow 7)$, $\epsilon_2(3\rightarrow 7)$, $\epsilon_2(4\rightarrow 7)$, $\epsilon_2(2\rightarrow 8)$, $\epsilon_2(3\rightarrow 8)$, ϵ_2 $(4\rightarrow 8)$, and $\epsilon_2(4\rightarrow 10)$. The fitting procedure used here has difficulty in reproducing the eigenvalues calculated by Christensen for the higher bands, particularly at L. To correct for these differences the sharp peaks of the $\epsilon_2(3\rightarrow 8)$ and $\epsilon_2(2\rightarrow 8)$ spectra should be shifted to lower energy by an amount of 0.9 eV, whereas the peak of the partial $\epsilon_2(4\rightarrow 10)$ spectrum should be shifted to higher energy by 1.4 eV. The result of these changes would be to spread out the intensity of the structures at 20.5 eV in Fig. 2 and to improve agreement with experiment. Even so, the theoretical structures are much sharper than those observed experimentally indicating the need to include lifetime broadening effects.

C. Summary

We list in Table II the energy positions of structures in experimental ϵ_2 data. The energy positions of theoretical structures are also listed, and are grouped according to our identifications with the experimental structures. Band pairs and, where possible, $\vec{k}$-space locations of the theoretical structures are indicated. It should be borne in mind that in many cases, the $\vec{k}$-space locations are only approximate and that the transitions take place over extended regions of $\vec{k}$ space around the stated location.

V. OTHER MODELS

The experimental data are compared in Fig. 7 with the results of a model having $\vec{k}$ conservation but constant matrix elements ($\bar{\epsilon}_2^d$, represented by short dashed curves) and a nondirect model ($\bar{\epsilon}_2^n$, also with constant matrix elements, and represented by the long dashed curves). The $\bar{\epsilon}_2^d$ and $\bar{\epsilon}_2^n$ results have been arbitrarily scaled to the experimental results. The comparison between the ϵ_2^d and $\bar{\epsilon}_2^d$ curves of Figs. 1 or 2 and Fig. 7 shows the influence of the matrix elements. Inclusion of the matrix elements, for example, reduces the structures at 1.3 and 4.6 eV in the case of Rh and at 1.2 and 7.5 eV in the case of Pd dramatically. In the region $\hbar\omega \geq 8$ eV these more approximate models give $\bar{\epsilon}_2^d$ and $\bar{\epsilon}_2^n$ values which are rather flat and which do not display the edge and plateau shown by ϵ_2^d and are seen also in experiment. On the oth-

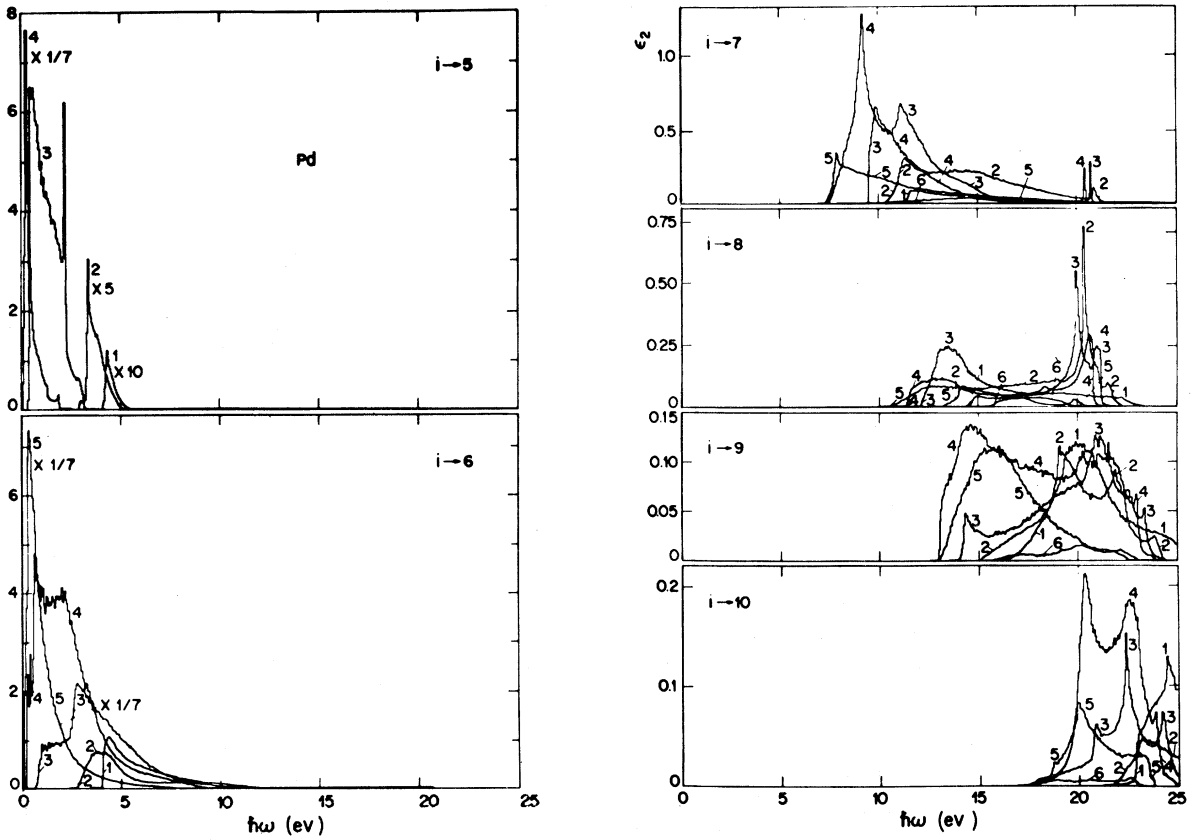

FIG. 6. Partial $\epsilon_2(i \rightarrow f)$ spectra of Pd for transitions from the initial band i into the final band f.

TABLE II. Locations in energy and $\vec{k}$ space of experimental and theoretical ϵ_2 structures.

	Rhodium				Palladium			
	Expt. (eV)	Theor. (eV)	Band pair $i \rightarrow f$	$\vec{k}$-space location	Expt. (eV)	Theor. (eV)	Band pair $i \rightarrow f$	$\vec{k}$-space location
Low	1.2				1.3			
	2.8	2.8	3→6	L,Σ				
		2.9	3→5	L				
Med	5.4	5.2	1→6	Σ	4.3	4.2	1→6	Σ
High	11.6	10.4	4→7	Q	10.0	9.3	4→7	Q
		10.8	3→7	U,X		9.9	3→7	L
						11.2	3→7	U,X
		12.5	2→7	W,Q				
	14.6	14.1	3→8	W	~15.0	13.5	3→8	Z
		18.4	2→8	Q,L		20.1	3→8	L
	19.3	18.3	3→8	L	~20.4	20.4	2→8	L
		18.6	4→8	Λ				
		20.4	2→9	X,Δ		20.4	4→10	L
		21.2	1→9	X,Δ		22.4	3→10	Q

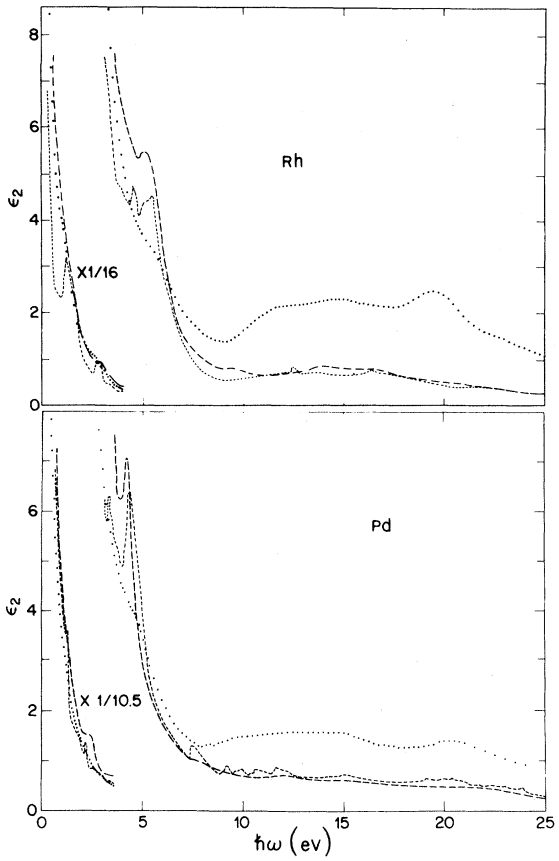

FIG. 7. Comparison of the calculated ϵ_2 results for Rh and Pd obtained using a model having $\underline{k}$ conservation but constant matrix elements (short dashed curves) and a model having nondirect transitions and also constant matrix elements (long dashed curves) with the experimental data (dots).

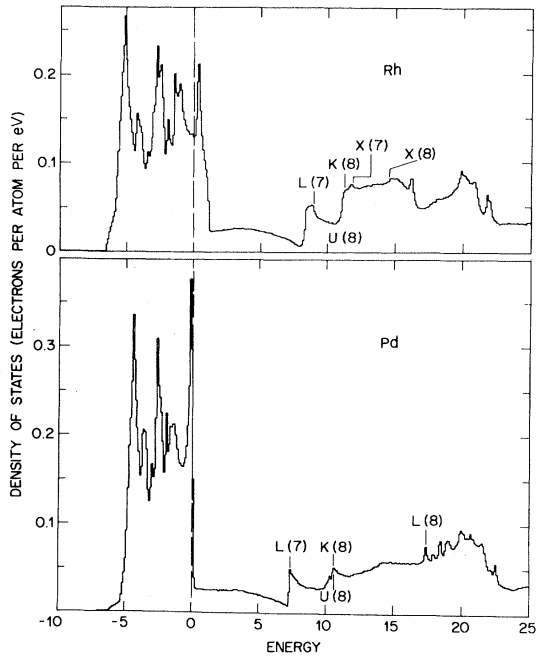

FIG. 8. Density of states of Rh (upper part) and Pd (lower part) calculated with the parameters of Table I.

er hand, the approximate models are successful in reproducing features at 2.9 and at 4.2 eV in Pd, which are present at very similar energies in the experimental data. The feature at 5.2 eV for Rh (4.2 eV for Pd) has been attributed to transitions between bands $1\rightarrow 6$ along Σ. In the case of $\bar{\epsilon}_2^n$ this feature arises through transitions to the Fermi level from the prominent density of states peak at the bottom of the d bands (see Fig.8). In Rh (Pd) this peak occurs at -5.2 (-4.4) eV relative to E_F. The 2.9-eV feature for Rh in ϵ_2^d and $\bar{\epsilon}_2^d$ arises from transitions from band 3 into band 5 (and, to a lesser extent, into band 6). In $\bar{\epsilon}_2^n$ the 2.9-eV feature arises through transitions from states in the sharp DOS peak at -2.6 eV to states in the peak just above E_F; this peak arises predominantly from band 3. Thus all three models are in agreement with regard to the source of the initial states for these features.

In conclusion, the approximate models can be quite useful in identifying experimental ϵ_2 structures, perhaps more useful than attempts to make identifications with critical-point structures at high-symmetry points in the Brillouin zone. A full understanding, however, requires a direct transition model with inclusion of momentum matrix elements. Good agreement with experiment is then obtained both with regard to positions and magnitudes of prominent structures. This leads to reliable identifications on $\vec{k}$-space locations and permits recommendations for empirical adjustments to the band structure.

ACKNOWLEDGMENT

We are grateful to J. H. Weaver for sending the numerical values of the experimental ϵ_2 data for Rh and Pd.

*Permanent address: Institut für Materialentwicklung IFF/KFA, D-517 Jülich, W. Germany.

[1]L. R. Windmiller, J. B. Ketterson, and S. Hornfeldt, Phys. Rev. B 3, 4213 (1971).
[2]J. H. Weaver, Phys. Rev. B 11, 1416 (1975), and references therein.
[3]J. F. Janak, D. E. Eastman, and A. R. Williams, Solid State Commun. 8, 271 (1970).
[4]M. M Traum and N. V. Smith, Phys. Rev. B 9, 1353 (1974).
[5]H. Höchst, S. Hüfner, and A. Goldmann, Phys. Lett. A57, 265 (1976).
[6]D. R. Lloyd, C. M. Quinn, and N. V. Richardson, Surf. Sci. 63, 174 (1977).
[7]N. Dahlbäck, P. O. Nilsson, and M. Pessa, Phys. Rev. B 19, 5961 (1979).
[8]H. Asonen, M. Lindroos, M. Pessa, and N. Dahlbäck, Solid State Commun. 35, 69 (1980).
[9]R. Podloucky, R. Lässer, E. Wimmer, and P. Weinberger, Phys. Rev. B 19, 4999 (1979).
[10]C. G. Olson, D. W. Lynch, and R. Rosei, Phys. Rev. B 22, 593 (1980).
[11]F. M. Mueller, A. J. Freeman, J. O. Dimmock, and A. M. Furdyna, Phys. Rev. B 1, 4617 (1970).
[12]O. K. Andersen, Phys. Rev. B 2, 883 (1970).
[13]G. S. Painter, J. S. Faulkner, and G. M. Stocks, Phys. Rev. B 9, 2448 (1974).
[14]N. E. Christensen, Phys. Rev. B 14, 3446 (1976).
[15]V. L. Moruzzi, J. F. Janak, and A. R. Williams, in *Calculated Electronic Properties of Metals* (Pergamon, New York, 1978), p. 144.
[16]J. H. Weaver and R. L. Benbow, Phys. Rev. B 12, 3509 (1975).
[17]J. H. Weaver and C. G. Olson, Phys. Rev. B 14, 3251 (1976).
[18]J. H. Weaver, C. G. Olson, and D. W. Lynch, Phys. Rev. B 15, 4115 (1977), and references therein.
[19]D. T. Pierce and W. E. Spicer, Phys. Status Solidi B 60, 689 (1973).
[20]N. E. Christensen, Phys. Status Solidi B 55, 117 (1973).
[21]W. Braun, M. Neumann, M. Iwan, and E. E. Koch, Phys. Status Solidi B 90, 525 (1978).
[22]G. Borstel, W. Braun, M. Neumann, and G. Seitz, Phys. Status Solidi B 95, 453 (1979).
[23]R. Lässer and N. V. Smith, Solid State Commun. 37, 507 (1981); R. Lässer, N. V. Smith, and R. L. Benbow, Phys. Rev. B 24, 1895 (1981).
[24]R. Lässer and N. V. Smith, Phys. Rev. B 24, 1910 (1981).
[25]N. V. Smith, Phys. Rev. B 19, 5019 (1979).
[26]J. Friedel, P. Lenglart, and G. Leman, J. Phys. Chem. Solids 25, 781 (1964); E. Abate and M. Asdente, Phys. Rev. 140, A1303 (1965); H. Ehrenreich and L. Hodges, in *Methods in Computational Physics,* edited by B. Alder (Academic, New York, 1968), Vol. 8, p. 149.
[27]E. I. Blount, in *Solid State Physics,* edited by F. Seitz and D. Turnbull (Academic, New York, 1962), Vol. 13, p. 305.
[28]W. E. Spicer, Phys. Rev. 154, 385 (1967).
[29]J. H. Weaver, C. Krafka, D. W. Lynch, and E. E. Koch, Z.A.E.D Phys. Daten (in press).
[30]J. F. Janak, A. R. Williams, and V. L. Moruzzi, Phys. Rev. B 11, 1522 (1975).
[31]R. Rosei, R. Lässer, N. V. Smith and R. L. Benbow, Solid State Commun. 35, 979 (1980); P. Heimann, H. Miosga, and H. Neddermeyer, *ibid.* 29, 463 (1979).